Journal of Materials Processing Technology 168 (2005) 464–470

Journal of Materials Processing Technology

www.elsevier.com/locate/jmatprotec

Grain growth control in Nb-doped $BaTiO_3$

E. Brzozowski, M.S. Castro *

Institute of Materials Science and Technology (INTEMA), CONICET-Universidad Nacional de Mar del Plata, Av. J.B. Justo 4302, B7608FDQ Mar del Plata, Argentina

Received 19 September 2003; received in revised form 13 January 2005; accepted 3 February 2005

Abstract

In this work, the grain growth inhibition effect of Nb_2O_5 on $BaTiO_3$ was improved by employing selected raw materials and an advanced milling technique. $BaTiO_3$ prepared from crystalline TiO_2 powder and needle-shaped $BaCO_3$ led to large grains on sintering, in addition to second phases due to Ti segregation and non-complete Nb incorporation. These phases did not inhibit grain growth but they affected the permittivity–temperature dependence of the material. In these materials, compensation charge mechanisms by electrons provided semiconducting characteristics at room temperature.

Further modifications on materials selection and ceramic processing varied the Nb incorporation extent significantly. Mechanochemically activated $BaCO_3$ reactant and ultrafine TiO_2 led to an early reaction. It provided a wide temperature range for Nb^{5+} incorporation as the $BaCO_3$–TiO_2 reaction progressed. Complete, homogeneous Nb incorporation in these materials allowed a strong grain growth inhibition on sintering and avoided accumulation of needle-shaped phases. Simultaneously to the grain growth inhibition phenomenon a considerable increase in titanium vacancy concentration was detected. Resulting materials stabilized in a pseudocubic phase and showed high dielectric features at room temperature.

Keywords: Powders–solid state reaction; Defects; Microstructure; Dielectric properties; $BaTiO_3$ and titanates

1. Introduction

Barium titanate and its solid solutions have been extensively used in many technical applications due to their ferroelectric properties [1–5]. Owing to the strong dependence of ferroelectric properties on grain size and compositional aspects, microstructural control has become very important [6]. It is well known that grain growth can be successfully controlled by the incorporation of small amounts of fine sized particles such us Nb_2O_5, Sb_2O_3, La_2O_3 and others [7–9]. Incorporation of donors above 0.3 mol% of additive oxide leads to an extraordinary change in $BaTiO_3$ properties. Below this doping threshold, coarse-grained $BaTiO_3$ becomes a semiconductor. On further dopant addition, $BaTiO_3$ ceramics show a fine-grained microstructure and insulating characteristics. This phenomenon, usually referred to as the "doping anomaly", is closely related to the microstructure and defect charge compensation modes [10]. Also, it was found that different doping styles modified the additive incorporation and the grain growth control [11,12].

Application of $BaTiO_3$ in ferroelectric devices requires a high density and homogeneous microstructure with grain sizes around 1 μm. The use of optimized powders and ceramic processing limit the second phase formation, impurity segregation or abnormal grain growth that usually degrades the material features [13]. On this matter, continual industrial effort is focused on improvement in the manufacturing process, so that many advances have been made with sophisticated technologies [14–16]. From the manufacturers viewpoint, an innovative technology should also provide a compromise between low cost process and reliable properties.

The use of an advanced milling step in the $BaTiO_3$ solid-state process remarkably enhances the grain size distribution, particle reactivity and further sinterability of the ceramic powder. On this matter, the high-energy milling is a conventional ball milling in which the mechanical energy activates chemical reactions at low temperatures [17–19].

* Corresponding author. Tel.: +54 23 816600; fax: +54 23 810046.
E-mail address: mcastro@fi.mdp.edu.ar (M.S. Castro).

0924-0136/$ – see front matter © 2005 Elsevier B.V. All rights reserved.
doi:10.1016/j.jmatprotec.2005.02.246

In this work, high-energy milling and optimized reactants have been used to improve traditional $BaCO_3$–TiO_2 solid-state synthesis, additive incorporation and particle sinterability. We established a link among processing variables and properties of $BaTiO_3$ ceramics. In addition to this, the microstructure and electrical properties of the final product were explained in terms of the ionic defect structure.

2. Experimental procedure

Three series of $BaTiO_3$-based materials were prepared from commercial $BaCO_3$ (Lennox Lab. Inc.), TiO_2 and Nb_2O_5 (Fluka A.G., Buchs S.G., medium particle size 1.8 μm) via the conventional mixed-oxide route. Two different TiO_2 reactants were alternatively used; that was a highly reactive, amorphous TiO_2 powder (Degussa P25, medium particle size 0.05 μm, referred to as F) and a crystalline, coarsened TiO_2 powder (Baker Chem. Co., medium particle size 0.64 μm, referred to as G). A standard $BaCO_3$ previously activated was employed. Activation of $BaCO_3$ powder was performed in isopropilic medium through high energy milling in a planetary mill with ZrO_2 balls for (A) 4 h (medium particle size 1.20 μm) or (B) 10 h (medium particle size 0.90 μm).

To ensure the complete reaction of the reactants at high temperature, a $BaCO_3$:TiO_2 ratio of 1:1.01 was chosen. To study the influence of processing modifications and raw materials on donor performance, an additive concentration of 0.15 mol% of Nb_2O_5 was fixed. TiO_2, $BaCO_3$ and Nb_2O_5 powders were mixed in isopropilic medium using a high-speed turbine at 6000 rpm for 5 min. Dried powders were thermally treated at 1150 °C for 2 h and sieved through a 100 μm mesh. The thermally treated powders were referred as P1–P3 (see Table 1).

Powders were uniaxially pressed into disks of 1 cm in diameter and 0.2 cm thick under 20 MPa without a binder or lubricant. Samples were sintered in air at 1350 °C for 3 h with a heating/cooling rate of 3 °C/min. Finally, electrodes were painted with an Ag–Pd paste.

Thermal events during thermal treatment were analyzed by differential thermal analysis (DTA) (Shimadzu DTA-50), with a heating rate of 3 °C/min up to 1000 °C. Density of the sintered samples was measured by Archimedes' Method with distilled water as fluid medium. X-ray diffraction analyses (XRD) were carried out on thermally treated and sintered samples using a Philips 1830, with Cu Kα radiation and Ni filter, at 40 kV and 30 mA. To quantify the cell distortion, tetragonality parameters (c/a) were calculated from the reflections of the (1 1 1) and (2 0 0) planes of sintered $BaTiO_3$. A scanning rate of 0.125°/min was used. Suitable surface for microstructural analysis was achieved by polishing the samples with SiC paper and diamond paste. Grain boundaries were highlighted in the polished surface through a thermal etching treatment at 1150 °C for 10–25 min. Etched samples were analyzed by scanning electron microscopy (SEM) using a Philips 505 microscope, while elemental analyses (EDS) were carried out with an EDAX (Topcon SM-300 and PGT digital spectrometer). By using the Soft Imaging System AnalySIS® 3.0 software, evaluation of the average grain size was performed on SEM images. Paramagnetic defects were determined by electron paramagnetic resonance (EPR) spectroscopy on sintered and ground samples, with a Bruker spectrometer (band *X*) using a gain of 2×10^4, a power of 5 dB and a modulation amplitude of 6.3 Gpp. For every EPR signal, the double integrated intensity (DII) was calculated as Murugaraj et al. reported in their article [20]. The DII gives the relative concentration of a given ionic defect in the perovskite lattice.

Electrical resistivity at room temperature (ρ_{RT}) was measured with a Keithley 614 Electrometer applying a dc-voltage of 10 V. Capacitance and loss tangent ($\tan\delta$) were recorded from 25 to 125 °C with a Hewlett Packard 4284A LCR meter, at 1 and 100 kHz. The real part of the dielectric permittivity (ε') was obtained from the measured capacitance.

Table 1
Nomenclature of the samples

Powder	$BaCO_3$ (milling hours)	TiO_2	Nb_2O_5 (mol%)	Nomenclature of the sintered sample
P1	4	F	0.15	S1
P2	10	F	0.15	S2
P3	4	G	0.15	S3

3. Results and discussion

In Fig. 1, the typical endothermic peak belonging to α → β transformation of $BaCO_3$ around 830 °C depicted the $BaCO_3$ amount remaining in the system at that temperature. $BaCO_3$ peaks were remarkably dependent on mechanochemical activation and titania reaction. In sample P3, $BaCO_3$ content still present at 830 °C was higher than in the systems P1 and P2, where the $BaCO_3$ decomposition began earlier. As consequence of the reaction delay in P3, there was a narrow temperature range for Nb_2O_5 incorporation while the $BaTiO_3$ lattice was built. Also, decomposition of slightly activated $BaCO_3$ followed by its reaction with large TiO_2 particles started at

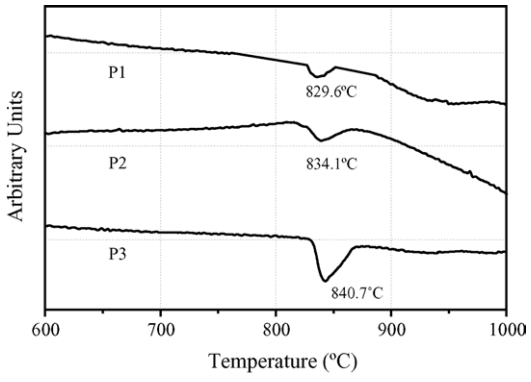

Fig. 1. DTA diagrams for P1–P3 powders prior to sintering.

Table 2
Characteristics of sintered samples S1–S3

Material	Density (%)	Grain size (μm)	Predominant structure	ρ (Ω cm)	ε_r	tan δ (%)
S1	81	5	Pseudocubic	$>10^8$	2200	1.6
S2	94	2	Pseudocubic	$>10^8$	2500	3.2
S3	95	>50	Tetragonal	44	300000	25

higher temperatures (780 °C, determined by XRD) than in P1 or P2. All thermally treated powders at 1150 °C for 2 h proved to be monophasic by XRD.

Samples S2 and S3 showed higher density values than S1 (Table 2). The different densification behavior was also reflected on microstructural characteristics. In Fig. 2, SEM photomicrographs of materials S1–S3 are shown. Homogeneous and fine-grained microstructures were observed in samples S1 and S2. A dramatic grain growth inhibition took place in sample S2. In S1, agglomeration of P1 powder (Fig. 3A) originated large pores on sintering, which were responsible for the density value observed in this ceramic (Fig. 3B and Table 2). In sample S3, needle-shaped second phases were homogeneously formed on sintering, however their formation did not hinder the grain growth. In fact, grains as large as 50 μm were observed. Needle-shaped phases were not observed in S1 and S2 materials sintered at 1350 °C for 2 h. In these cases, EDS analyses performed on non-etched samples revealed the presence of a Ti rich-phase covering the grains. According to EDS analyses, composition of the second phases was close to $Ba_6Ti_{17}O_{40}$ (in S1 and S2 materials) and $Ba_6Ti_{14}Nb_2O_{39}$ (in S3).

In all cases, sintering behavior was strongly dependent on $BaTiO_3$ powder characteristics, which were as expected dependent on the solid-state synthesis. From a previous work [21], significant differences between TiO_2 and $BaCO_3$ granulometry in P1 led to TiO_2 particle agglomerates (Fig. 3A). In addition, employment of typical needle-shaped $BaCO_3$ slightly activated ($BaCO_3$ in P1) and round-shaped TiO_2 resulted in a rather difficult mixing process [22]. Agglomerated TiO_2 particles in P1 (Fig. 3A) could sinter themselves at the beginning of the thermal treatment. As far as $BaCO_3$ decomposed [21], reaction between BaO and TiO_2 in P1 took place on the external layers of the agglomerates. Finally, BaO diffusion into the TiO_2 agglomerates allowed a complete reaction, thus a monophasic-based $BaTiO_3$ product was obtained. Since morphology and particle size of TiO_2 powder determine those of the $BaTiO_3$, a coarsened powder product was

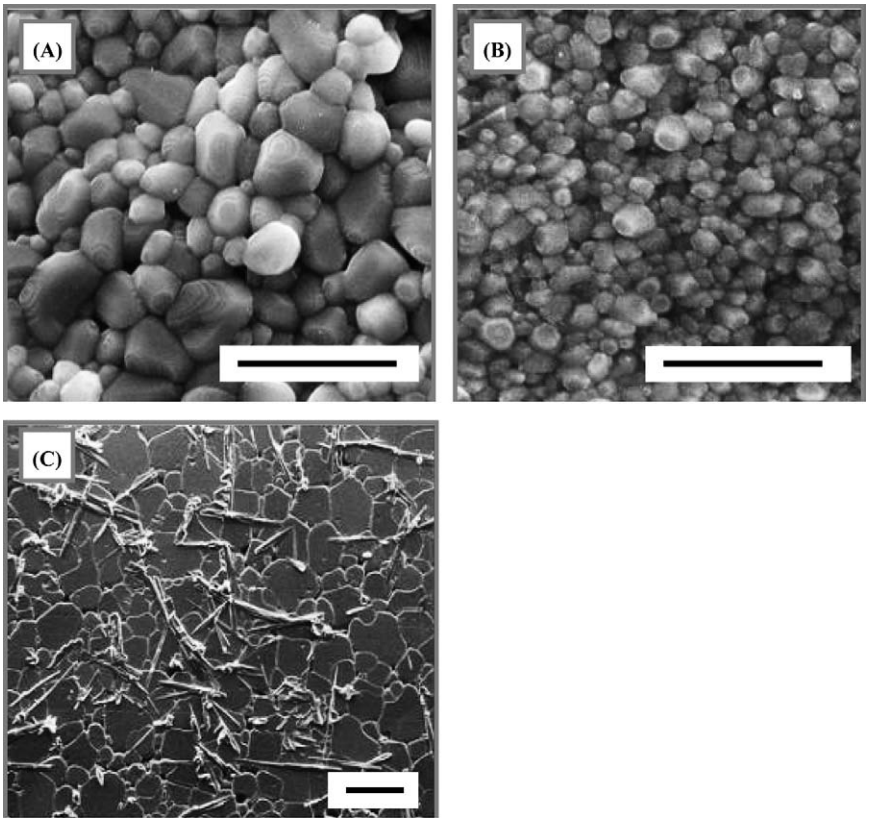

Fig. 2. SEM photomicrographs for S1 (A), S2 (B) and S3 (C) materials. Bar = 10 μm (S1 and S2 samples), and bar = 100 μm (S3 sample).

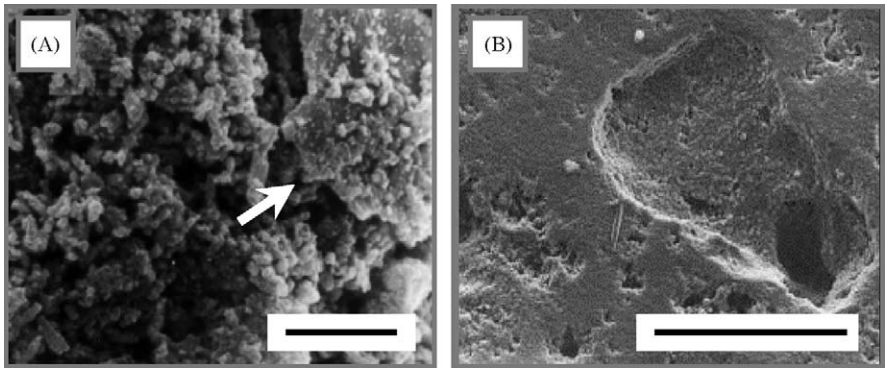

Fig. 3. (A) TiO_2 agglomerate in P1 mixture, bar = 10 μm. (B) Detail of large pore on S1 material, bar = 100 μm.

obtained (P1). On sintering, coarsened $BaTiO_3$ particles led to higher grain size and a substantial lower density (S1) than the expected without agglomeration (S2).

It is well known that grain growth extent in Nb-doped materials depends on Nb_2O_5 concentration [10,23,24]. However, results in our materials indicated different grain growth for identical Nb doping (Fig. 2). It is likely that granulometry and reactivity of TiO_2 and $BaCO_3$ also influenced the Nb incorporation on sintering $BaTiO_3$. Explanation arises by considering the Nb fraction incorporated at the beginning of the solid-state reaction between $BaCO_3$ and TiO_2. Rigorous activation of $BaCO_3$ in P2 impelled $BaCO_3$ decomposition and a subsequent reaction with TiO_2 at very low treatment temperatures (630 °C, determined by XRD). Early incorporation of Nb additive in P2 enabled its grain growth inhibition effect on sintering. Thus, fine-grained ceramics were obtained (S2). In addition to this, originally large TiO_2 particles contributed also to the development of large $BaTiO_3$ grains in this sample.

In S1 and S2 materials, tetragonal–cubic transformation was blocked as consequence of grain refinement. Thus, the structure became pseudocubic (Fig. 4) instead of purely tetragonal. In S3, tetragonal structure split up into two peaks, as corroborated in Fig. 4 and Table 2. Samples S1 and S2 showed higher resistivities than S3 due to the presence of a higher amount of intergranular barriers. Also, tetragonal phase stabilization in sample S3 favored dominion formation, and the cancellation of intergranular barriers. In this sample a PTCR behavior is observed.

It is known that, the incorporation of Nb^{5+} ions at the B-sites of the $BaTiO_3$ perovskite lattice originated a charge excess to be compensated [25]. Compensation mechanisms depended on the Nb^{5+} concentration added. For small Nb^{5+} concentrations, electronic compensation should prevail as follows [24,25]:

$$2BaO + Nb_2O_5 \rightarrow 2Ba_{Ba} + 2Nb^{\bullet}{}_{Ti} + 6O_O + \tfrac{1}{2}O_2(g) + 2e' \quad (1)$$

simultaneously:

$$Ti^{4+} + 1e' \rightarrow Ti^{3+} \quad (2)$$

When a large number of Nb^{5+} ions were incorporated into the lattice, charge disequilibria were compensated by ionic defects. In our system (Ba/Ti < 1):

$$BaO + Nb_2O_5 \rightarrow Ba_{Ba} + V''_{Ba} + 2Nb^{\bullet}{}_{Ti} + 6O_O \quad (3)$$

$$V''_{Ba} \rightarrow V'_{Ba} + 1e' \quad (4)$$

$$6BaO + 3Nb_2O_5 \rightarrow 6Ba_{Ba} + V''_{Ba} + 6Nb^{\bullet}{}_{Ti} + V''''{}_{Ti} + 21O_O \quad (5)$$

$$5BaO + 2Nb_2O_5 \rightarrow 5Ba_{Ba} + 4Nb^{\bullet}{}_{Ti} + V''''{}_{Ti} + 15O_O \quad (6)$$

$$2BaO + 2Nb_2O_5 + 3BaTiO_3 \rightarrow 5Ba_{Ba} + 4Nb^{\bullet}{}_{Ti} + V''''{}_{Ti} + 15O_O + 3TiO_2 \quad (7)$$

EPR analysis performed on S1–S3 showed two paramagnetic signals at $g = 2.004$ and 1.974 and six sharp resonance peaks

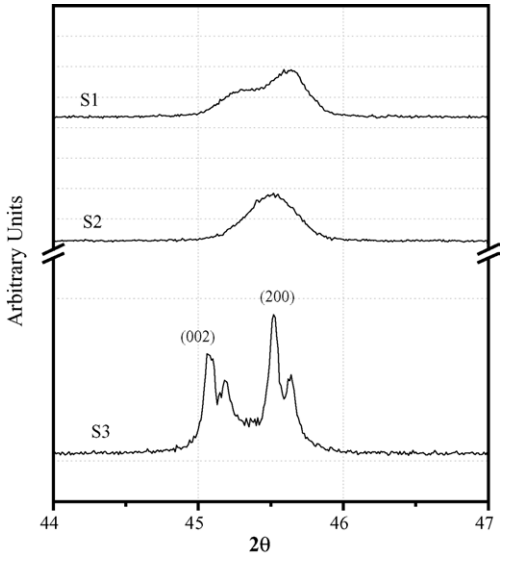

Fig. 4. XRD signals for S1–S3 materials.

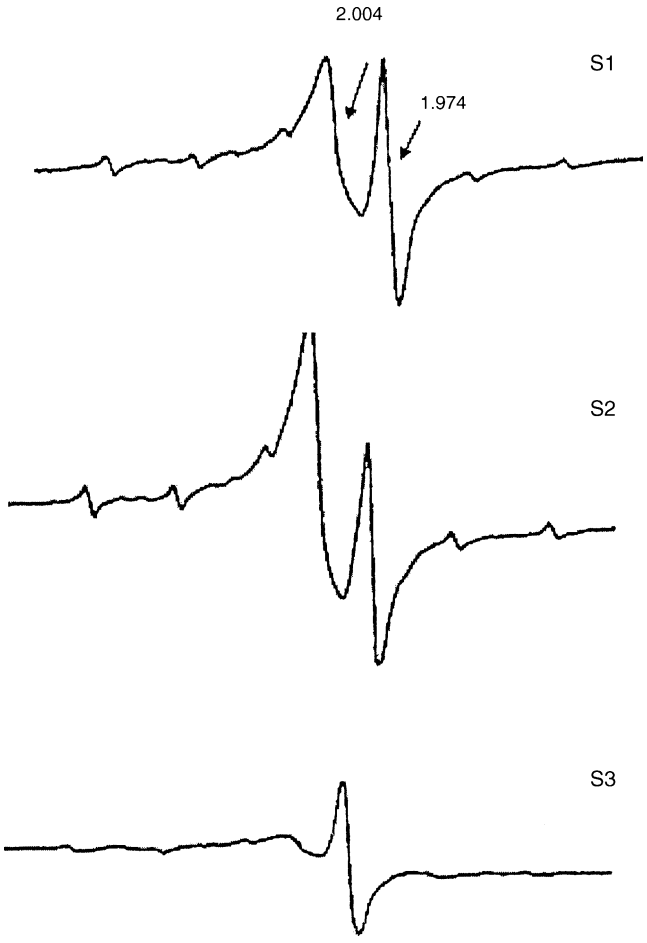

Fig. 5. EPR spectra of S1–S3 samples.

due to the hyperfine splitting of the ^{55}Mn isotope having a nuclear spin of 5/2 (Fig. 5). Kolodiazhnyi and Petric [26] related the EPR singlets with $g = 2.004$ and 1.974 to V_{Ti} (V'_{Ti} or V'''_{Ti}) and V'_{Ba}, respectively. The EPR signal at $g = 1.932$ attributed to Ti^{3+}, Ti^{3+}–V_O or Ti^{3+}–V_O–K(Na) [27] was not detected in these experiments. V'_{Ba} and V_{Ti} relative concentration determined by EPR depicted Nb^{5+} incorporation semiquantitatively. Table 3 suggests that Eqs. (5)–(7) prevailed for S1 and S2. Major incorporation of Nb ions followed by a titanium vacancy regime led to high-resistivity characteristics in S1 and S2 materials (Tables 2 and 3). Non-complete Nb incorporation in S3 led to electronic and barium vacancies compensation regimes (Eqs. (1) and (3)), in detriment of titanium vacancies formation (Table 3). Electrons passing to the conduction band compensated the charge excess introduced

Table 3
DII values correspondent to barium and oxygen vacancies detected by EPR in samples S1–S3

Material	DII-V_{Ti}	DII-$V^{\bullet}_{Ba}$
S1	12.7	2.1
S2	18.6	1.0
S3	0.3	1.2

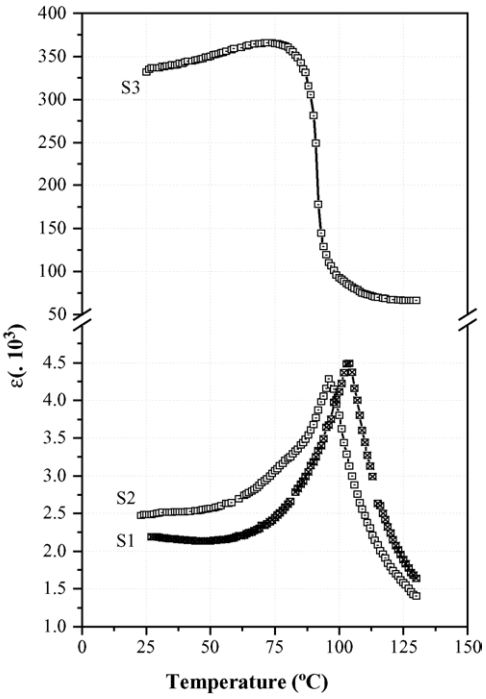

Fig. 6. Real part of the dielectric permittivity vs. temperature dependence at 1 kHz for S1–S3 materials.

by doping, so the electrical resistivity decreased and the loss tangent increased as was experimentally confirmed (Table 2). Evidence of Ti^{3+} (Eq. (2)) was also provided by the blue color of the sintered S3 materials [28].

According to EPR and microstructural results, titanium vacancies, formed by niobium replacement in the $BaTiO_3$ lattice, played a dominant role in grain growth control. Ionic defects piled up at grain boundaries and decreased grain boundary mobility [29]. On the other hand; Ti-rich secondary phases resulted from Ti segregation from a monophasic $BaTiO_3$, as consequence of Nb incorporation (see Eq. (7)).

Fig. 6 shows permittivity versus temperature curves for S1–S3 materials in the temperature range between 25 and 125 °C at 1 kHz. Two different responses were observed. On one hand, S1 and S2 materials showed a typical Curie-Weiss behavior with a cubic–tetragonal transition at 104 and 95 °C, respectively. On the other hand, the permittivity peak at the Curie temperature was suppressed in sample S3, with nearly flat temperature dependence in the range between 25 and 95 °C. However, when a frequency of 100 kHz was applied, a characteristic Curie–Weiss response in S3 with a transition temperature at 106 °C (Fig. 7) was observed. This interesting frequency dependence feature has scarcely been reported for $BaTiO_3$ materials. A qualitative explanation comes up on considering the different polarization forms leading to given permittivity features, in dependence on the driving frequency of the electric field. There are a number of relaxation effects depending on frequency and temperature described in the literature [30]. In materials like S3 where at least two phases

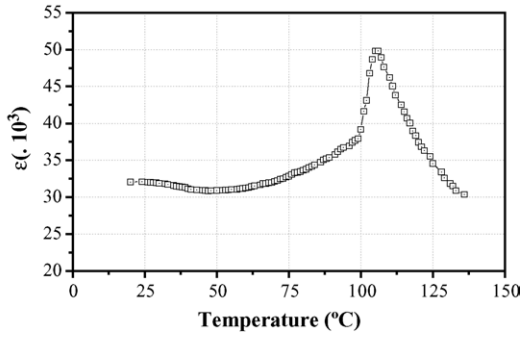

Fig. 7. Real part of the dielectric permittivity vs. temperature dependence at 100 kHz for S3 material.

coexist, interfacial polarization could be associated to the movement of free charges across a potential barrier separating two phases under the effect of an electric field. In such a case, movement of free charges through long distances compared with molecular distances requires a long time to relax, therefore the process is only possible at low frequencies [30,31]. When the temperature is changed the dipole polarization is influenced [32]. It is known that two cases are possible: (a) for higher temperatures it will be more difficult to orient the dipoles by the applied field due to the thermal agitation energy, and (b) the higher the temperature the higher the density of dipoles available contributing to the total polarization. This dielectric relaxation, which obeys an Arrhenius type thermal activation law, partially masks the ferroelectric–paraelectric transition at low frequencies. At higher frequencies the influence of the relaxation process on the relative permittivity was reduced and a ferroelectric–paraelectric transition peak was observed.

4. Conclusions

Reactant characteristics and ceramic processing played a decisive role on Nb incorporation into the $BaTiO_3$ lattice. That dependence was also observed in relation to the defect structure at room temperature. Experimental results disclosed that titanium vacancies depended on the TiO_2 granulometry and $BaCO_3$ milling time. Charged titanium vacancies could be associated with impurities at the grain boundaries. The moving boundary must drag along the defects, thus retarding grain growth.

In materials with a low Nb^{5+} incorporation, needle-shaped second phases were spread over a wide bulk area and they did not inhibit grain growth on sintering. In such case, electronic compensation mechanisms allowed the boundary mobility to approach a maximum. Then, large grains were developed on sintering.

In materials with high Nb^{5+} incorporation, high amount of titanium vacancies was developed. These vacancies contributed to grain growth inhibition on sintering.

Electrical properties were closely related with the compensating defect mode induced by additive incorporation. Also, additive incorporation was strongly dependent on raw materials and processing. Optimization of milling technology and appropriate reactant selection modified the additive effect to achieve desired features for dielectric or semiconductor devices.

Acknowledgement

Support of this work was provided by Fundación Antorchas, CONICET, as well as Universidad Nacional de Mar del Plata.

References

[1] J. Qi, Z. Gui, Y. Wang, Q. Zhu, Y. Wu, L. Li, The PTCR effect in $BaTiO_3$ ceramics modified by donor dopant, Ceram. Int. 28 (2002) 141–143.
[2] S.F. Wang, T.Y.K. Yang, Y.R. Wang, Y. Kuromitsu, Effect of glass composition on the densification and dielectric properties of $BaTiO_3$ ceramics, Ceram. Int. 27 (2001) 157–162.
[3] G.H. Jonker, Equilibrium barriers in PTC thermistors, in: L.M. Levinson (Ed.), Advances in Ceramics, vol. 1, American Ceramic Society, Columbus, OH, 1981, pp. 155–166.
[4] M.T. Buscaglia, V. Buscaglia, M. Viviani, P. Nanni, M. Hanuskova, Influence of foreign ions on the crystal structure of $BaTiO_3$, J. Eur. Ceram. Soc. 20 (2000) 1997–2007.
[5] B.D. Stojanovic, C.R. Foschini, M.A. Zaghete, F.O.S. Viera, K.A. Peron, M. Cilense, J.A. Varela, Size effect on structure and dielectric properties of Nb-doped barium titanate, J. Mater. Process. Technol. 143–144 (2003) 802–806.
[6] D. Makovec, N. Ule, M. Drofenik, Positive temperature coefficient of resistivity effect in highly donor-doped barium titanate, J. Am. Ceram. Soc. 84 (2001) 1273–1280.
[7] F.D. Morrison, D.C. Sinclair, A.R. West, Characterization of lanthanum-doped barium titanate ceramics using impedance spectroscopy, J. Am. Ceram. Soc. 84 (2001) 531–538.
[8] M. Drofenik, Origin of the grain growth anomaly in donor-doped barium titanate, J. Am. Ceram. Soc. 76 (1993) 123–128.
[9] M.H. Lin, H.Y. Lu, Densification retardation in the sintering of La_2O_3-doped barium titanate ceramic, Mat. Sci. Eng. A 323 (2002) 167–176.
[10] M.N. Rahaman, M. Manalert, Grain boundary mobility of $BaTiO_3$ doped with aliovalent cations, J. Eur. Ceram. Soc. 18 (1998) 1063–1071.
[11] J. Qi, L. Li, W. Li, Y. Wang, Z. Gui, Synthesis of nanocrystalline manganite powders via a gel auto-combustion process for NTC thermistor applications, Mater. Sci. Eng. B 99 (2003) 217–220.
[12] Y. Yuan, S. Zhang, W. You, Preparation of $BaTiO_3$-based X7R ceramics with high dielectric constant by nanometer oxides doping method, Mater. Lett. 58 (2004) 1959–1963.
[13] E. Brzozowski, M.S. Castro, C.R. Foschini, B. Stojanovic, Secondary phases in Nb-doped $BaTiO_3$ ceramics, Ceram. Int. 28 (2002) 773–777.
[14] A. Lewis, Colloidal processing of ceramics, J. Am. Ceram. Soc. 83 (2000) 2341–2359.
[15] B.L. Newalkar, S. Komarneni, H. Katsuki, Microwave-hydrothermal synthesis and characterization of barium titanate powders, Mater. Res. Bull. 36 (2001) 2347–2355.
[16] J.F. Bocquet, K. Chor, C. Pommier, Barium titanate powders synthesis from solvothermal reaction and supercritical treatment, Mater. Chem. Phys. 57 (1999) 273–280.

[17] B.D. Stojanovic, V.B. Pavlovic, V.P. Pavlovic, S. Djuric, B.A. Marinkovic, M.M. Ristic, Dielectric properties of barium-titanate sintered from tribophysically activated powders, J. Eur. Ceram. Soc. 19 (1999) 1081–1083.
[18] E. Brzozowski, M.S. Castro, Lowering the synthesis temperature of high-purity $BaTiO_3$ powders by modifications in the processing conditions, Thermochim. Acta 398 (2003) 123–131.
[19] J. Xue, J. Wang, D. Wan, Nanosized barium titanate powder by mechanical activation, J. Am. Ceram. Soc. 83 (2000) 232–234.
[20] P. Murugaraj, T.R.N. Kutty, M. Subba Rao, Diffuse phase transformations in neodymium-doped $BaTiO_3$ ceramics, J. Mater. Sci. 21 (1986) 3521–3527.
[21] E. Brzozowski, M.S. Castro, Synthesis of barium titanate improved by modifications on the kinetic of the solid state reaction, J. Eur. Ceram. Soc. 20 (2000) 2347–2351.
[22] D.F.K. Hennings, B.S. Schreinemacher, H. Schreinemacher, Solid-state preparation of $BaTiO_3$-based dielectrics, using ultrafine raw materials, J. Am. Ceram. Soc. 84 (2001) 2777–2782.
[23] T.B. Wu, N.J. Lin, Transition of compensating defect mode in niobium doped barium titanate, J. Am. Ceram. Soc. 77 (1994) 759–764.
[24] T. Hayashi, Preparation and properties of niobium oxide coated barium titanate composite powders, Met. Powder Rep. 52 (1997) 40.
[25] H. Chan, M.P. Harmer, D. Smyth, Compensating defects in highly donor-doped $BaTiO_3$, J. Am. Ceram. Soc. 69 (1986) 507–510.
[26] T. Kolodiazhnyi, A. Petric, Analysis of point defects in polycrystalline $BaTiO_3$ by electron paramagnetic resonance, J. Phys. Chem. Solids 64 (2003) 953–966.
[27] R. Scharfschwerdt, A. Mazur, O.F. Schimer, H. Hesse, S. Mendricks, Oxygen vacancies in $BaTiO_3$, Phys. Rev. B 54 (1996) 15284–15290.
[28] B.-S. Chiou, S.-T. Lin, EPR evidence for compensating defects in $BaTiO_3$ grain boundary barrier layer capacitors, Mater. Chem. Phys. 24 (1990) 239–245.
[29] M.N. Rahaman, Grain growth of $BaTiO_3$ doped with aliovalent cations, in: K.M. Nair, A.S. Bhalla (Eds.), Ceramic Transactions, vol. 100, American Ceramic Society, Columbus, OH, 1999, pp. 23–32.
[30] J.M. Alabella Martin, J.M. Martínez Duart (Eds.), Física de dieléctricos, Marcombo S.A., Barcelona, Spain, 1984, p. 100.
[31] P.Q. Mantas, Dielectric response of materials: extension to the Debye model, J. Eur. Ceram. Soc. 19 (1999) 2079–2086.
[32] C. Elissalde, J. Ravez, Ferroelectric ceramics: defects and dielectric relaxations, J. Mater. Chem. 11 (2001) 1957–1967.